POLITECNICO DI TORINO
Repository ISTITUZIONALE

Convergence of a Spherical Multipole Expansion for Propeller Tonal Noise

Original
Convergence of a Spherical Multipole Expansion for Propeller Tonal Noise / Fruncillo, F., Capitani, G., Giannetti, F., Avallone, F., Luchini, P.. - (2026). (32nd AIAA/CEAS Aeroacoustics Conference (2026) Brussels (BEL) 26-29 May 2026) [10.2514/6.2026-3598].

Availability:
This version is available at: 11583/3011187 since: 2026-06-15T09:31:48Z

Publisher:
American Institute of Aeronautics and Astronautics

Published
DOI:10.2514/6.2026-3598

Terms of use:

This article is made available under terms and conditions as specified in the corresponding bibliographic description in the repository

Publisher copyright
AIAA preprint/submitted version e/o postprint/Author's Accepted Manuscript

(Article begins on next page)

16 October 2026

Convergence of a Spherical Multipole Expansion for Propeller Tonal Noise

F. Fruncillo*[1,2], G. Capitani†[1], F. Giannetti‡[1], F. Avallone§[3], and P. Luchini¶[1]
[1]*Università degli Studi di Salerno, Via Giovanni Paolo II, 132, Fisciano, 84084, Italy*
[2]*CIRA, Italian Aerospace Research Center, Via Maiorise, Capua, 81043, Italy*
[3]*Politecnico di Torino, Corso Duca degli Abruzzi, 24, Torino, 10129, Italy*

We examine an observer-independent framework for the prediction and validation of hovering propeller tonal noise, based on a spherical multipole expansion. The formulation separates source and observer dependence, so that the multipole coefficients are evaluated only once, and the acoustic field can then be reconstructed at any arbitrary observer locations at negligible additional cost. The convergence of the truncated series is assessed locally in both near- and far-field regions for three rotational speeds. The results show that only a modest number of terms is required for accurate predictions and that, for the operating conditions considered here, the first two terms are already sufficient in the far field. Validation against measurements shows good agreement for the first blade-passing harmonic over the full microphone arc, with mean errors lower than 1 dB. A Monte Carlo analysis is also performed to quantify the effect of uncertainty in the aerodynamic, geometric, and operating inputs. The predicted uncertainty bands confirm both the accuracy and the robustness of the proposed formulation.

I. Nomenclature

a_s	=	speed of sound
A_{lm}	=	multipole coefficient of degree l for harmonic m
$A_{D_{lm}}$	=	drag-related contribution to A_{lm}
$A_{L_{lm}}$	=	lift-related contribution to A_{lm}
$A_{T_{lm}}$	=	thickness-related contribution to A_{lm}
$A_{T'_{lm}}$	=	induced thickness-related contribution to A_{lm}
A_s	=	dimensionless sectional area
$B_{L_{lm}}$, $B_{D_{lm}}$	=	equatorial coefficients associated with the lift and drag contributions
$B_{T_{lm}}$, $B_{T'_{lm}}$	=	equatorial coefficients associated with the thickness and induced-thickness contributions
c	=	local blade chord
c_l, c_d	=	sectional lift and drag coefficients
C_{lm}	=	normalization constant of the spherical harmonics
E	=	airfoil efficiency
h_l	=	spherical Hankel function of the first kind and order l
j_l	=	spherical Bessel function of the first kind and order l
k_m	=	acoustic wavenumber of the m-th harmonic
l	=	multipole degree
l_{corr}	=	correlation length
l_{max}	=	maximum multipole degree retained in the truncated expansion
$l_{\text{max,ref}}$	=	maximum multipole degree for the reference solution
$l_{\text{max}}^{\text{req}}$	=	minimum truncation degree required to satisfy the prescribed convergence tolerance

*Researcher, Università degli Studi di Salerno, ffruncillo@unisa.it
†Researcher, Università degli Studi di Salerno, g.capitani1@studenti.unisa.it
‡Professor, Fluid Dynamics, Università degli Studi di Salerno, fgiannetti@unisa.it
§Professor, Aerodynamics, Politecnico di Torino, francesco.avallone@polito.it
¶Professor, Fluid Dynamics, Università degli Studi di Salerno, luchini@unisa.it

$L_{p,m}$	=	sound pressure level of the m-th harmonic
m	=	harmonic index
M_t	=	tip Mach number
n	=	rotational speed
n_o	=	number of observer locations
n_r	=	number of radial integration points
n_{req}	=	minimum number of retained multipole terms required to satisfy the prescribed convergence tolerance
N	=	number of blades
N_m	=	number of microphones used in the experimental comparison
N_{MC}	=	number of Monte Carlo runs
$p(\mathbf{x}_0, t)$	=	real acoustic pressure at observer position $\mathbf{x}_0$ and time t
$p_m(\mathbf{x}_0)$	=	complex pressure coefficient of the m-th harmonic at observer position $\mathbf{x}_0$
$p_m^{(l_{\max})}(\mathbf{x}_0)$	=	truncated approximation of the m-th harmonic obtained by retaining terms up to degree $l_{\max}$
$p_m^{\text{ref}}(\mathbf{x}_0)$	=	reference value of the m-th harmonic obtained with a sufficiently large truncation order
$p_{m,\text{rms}}$	=	root-mean-square pressure associated with the real m-th harmonic
p_{ref}	=	reference pressure for SPL, equal to $20\,\mu$Pa
P_{lm}	=	associated Legendre polynomial of degree l and order m
R	=	propeller tip radius
R_{hub}	=	hub radius
$\bar{R}_{\text{hub}}$	=	hub-to-tip ratio
r, θ, ϕ	=	spherical coordinates of the source position
r_0, θ_0, ϕ_0	=	spherical coordinates of the observer position
$\bar{r}$	=	normalized radial coordinate, $\bar{r} = r/R$
$\bar{r}_0$	=	normalized observer distance, $\bar{r}_0 = r_0/R$
t	=	time
Y_{lm}	=	spherical harmonic of degree l and order m
$\mathbf{x}_0$	=	observer position vector
$\varepsilon_m^{(l_{\max})}$	=	convergence error of the truncated m-th harmonic relative to the reference solution
ε_{tol}	=	prescribed convergence tolerance
γ	=	chord-to-diameter ratio
ϕ_s'	=	source azimuthal phase angle along the lifting line
φ_i	=	induced-flow angle at the blade section
ρ	=	air density
σ_v	=	relative standard deviation of the spanwise variable v
τ_c	=	computational speed-up
ω_m	=	angular frequency of the m-th harmonic
Ω	=	angular velocity of the propeller
BPF	=	blade-passing frequency
MAE	=	mean absolute error
RMSE	=	root-mean-square error
SPL	=	sound pressure level

II. Introduction

Predicting the tonal sound radiated by a propeller often requires evaluating the acoustic field at a large number of observer locations. This is the case, for example, when computing directivity patterns, microphone-array maps, or acoustic fields over extended spatial grids. In most available formulations [1–3], the observer coordinates remain embedded in the source integrals, so the acoustic pressure must be recomputed for every microphone position. While this is not a major issue when only a few observers are considered, it quickly becomes expensive when dense observer distributions are required. A recent formulation based on a spherical multipole expansion [4] of Goldstein acoustic analogy [5] addresses this limitation by separating source and observer dependence. In that framework,

the source-dependent quantities are collected into multipole coefficients that depend only on blade geometry and aerodynamic loading, whereas the observer coordinates appear only in the reconstruction of the acoustic field. As a result, the source integrals are evaluated once and then reused for any number of microphone locations. This feature makes the approach particularly attractive for applications in which the acoustic field must be evaluated repeatedly over large observer sets. The main drawback is that the benefit depends on the convergence of the truncated multipole series: the method is advantageous only if accurate predictions are obtained with a limited number of retained terms.

The objective of the present work is therefore to assess the practical performance of this formulation for the prediction of propeller tonal noise. In particular, this work addresses how rapidly the multipole series converges and in which regions of space a low-order truncation remains sufficient. Answering these questions is essential to use the approach as an efficient predictive tool rather than only as a formal representation of the acoustic field. The analysis is carried out for a hovering propeller. The multipole formulation is applied to large sets of observer locations and then the convergence of the acoustic field is examined by progressively increasing the truncation order of the series. This makes it possible to identify the regions in which the expansion converges rapidly and those in which a larger number of terms is required. Finally, the numerical predictions are compared with measurements taken from the literature [6]. Since some of the relevant inputs are not known with high accuracy, uncertainties in blade geometry, aerodynamic quantities, and operating conditions are propagated through a Monte Carlo analysis to estimate their effect on the sound pressure level (SPL) at the microphones.

III. Formulation

In an earlier work [7], the multipole expansion approach was applied to a propeller modelled as a lifting surface. In that case, the problem was reduced to a half-plane one and the Kirchhoff-Helmholtz integral was evaluated in closed form by means of tailored Green's functions [8]. That formulation proved effective and computationally efficient, but its underlying geometric approximation becomes less representative when the blade pitch angle is large. In such cases, the relevant loading and thickness effects are not fully captured by a planar distribution over the rotor disk, and a model based on a lifting line becomes more appropriate [9]. The main idea remains the same as in the previous multipole approach: the dependence on the observer position is isolated from the source terms, so that the latter can be computed once and then reused to reconstruct the acoustic field at arbitrary locations. In the lifting-line setting, the blade chord c is assumed to be small compared with the propeller diameter $2R$, so that each blade can be represented as a line source carrying the dominant aerodynamic and thickness-related effects. A more detailed derivation of the resulting expressions is reported in [4].

For a hovering lifting line lying in the plane of rotation $\theta = \pi/2$, the multipole coefficient A_{lm} associated with the m-th harmonic can be decomposed into four contributions

$$
\begin{aligned}
A_{L_{lm}} =& i\rho a_s^2 M_t^3 N m B_{L_{lm}} \int_{\bar{R}_{\text{hub}}}^{1} j_l\left(mM_t\bar{r}\right) \frac{\gamma c_l}{\cos\varphi_i}\left(1-\frac{\tan\varphi_i}{E}\right)\bar{r}e^{-im\phi_s'}d\bar{r} \\
A_{D_{lm}} =& \rho a_s^2 M_t^3 N m^2 B_{D_{lm}} \int_{\bar{R}_{\text{hub}}}^{1} j_l\left(mM_t\bar{r}\right) \frac{\gamma c_l \tan\varphi_i}{\cos\varphi_i}\left(1+\frac{1}{E\tan\varphi_i}\right)\bar{r}e^{-im\phi_s'}d\bar{r} \\
A_{T_{lm}} =& -4i\rho a_s^2 M_t^3 N m^3 B_{T_{lm}} \int_{\bar{R}_{\text{hub}}}^{1} j_l\left(mM_t\bar{r}\right) \gamma^2 A_s e^{-im\phi_s'}d\bar{r} \\
A_{T'_{lm}} =& -4\rho a_s^2 M_t^3 N m^2 B_{T'_{lm}} \int_{\bar{R}_{\text{hub}}}^{1} j_l\left(mM_t\bar{r}\right) \gamma^2 A_s \tan\varphi_i e^{-im\phi_s'}d\bar{r}
\end{aligned}
\tag{1}
$$

so that

$$
A_{lm} = A_{L_{lm}} + A_{D_{lm}} + A_{T_{lm}} + A_{T'_{lm}}
$$

Here j_l denotes the spherical Bessel function of the first kind and order l; c_l is the sectional lift coefficient; E is the airfoil efficiency, defined as $E = c_l/c_d$ where c_d is the sectional drag coefficient; and A_s is the dimensionless sectional area, defined as the actual sectional area divided by c^2. The tip Mach number is denoted by M_t, N is the number of blades, and ϕ_s' is the source phase angle along the blade. The integration variable $\bar{r} = r/R$ is the radial coordinate normalized by the propeller radius, and $\bar{R}_{\text{hub}}$ denotes the hub radius in the same normalized form. The four terms in Eq. (1) represent the distinct physical mechanisms retained by the lifting-line model. More specifically, the contributions $A_{L_{lm}}$ and $A_{D_{lm}}$ are associated with aerodynamic loading, mainly to lift and drag respectively, whereas $A_{T_{lm}}$ and $A_{T'_{lm}}$ arise from blade thickness and enter as higher order contributions in the small parameter $\gamma = c/2R$. All

symbols appearing in Eq. (1) are defined in the nomenclature. The quantities c_l, φ_i, E, and A_s are assumed to be known from the aerodynamic and geometric description of the propeller. The angular behaviour of each term is contained in the equatorial coefficients

$$B_{L_{lm}} = B_{T'_{lm}} = \left.\frac{dY^*_{lm}(\theta,0)}{d\theta}\right|_{\theta=\frac{\pi}{2}}, \qquad B_{D_{lm}} = B_{T_{lm}} = Y^*_{lm}\left(\frac{\pi}{2},0\right) \tag{2}$$

written in terms of the spherical harmonics Y_{lm}, defined as

$$Y_{lm}(\theta,\phi) = C_{lm}P_{lm}(\cos\theta)\, e^{im\phi}, \qquad C_{lm} = \sqrt{\frac{2l+1}{4\pi}\frac{(l-m)!}{(l+m)!}}$$

where P_{lm} are the associated Legendre polynomials. The symmetry properties of the four contributions are embedded in Eq. (2) and are worth noting. The $A_{L_{lm}}$ and $A_{T'_{lm}}$ terms are antisymmetric with respect to the rotor plane and therefore the pressure fields associated with them vanish on that plane. By contrast, $A_{D_{lm}}$ and $A_{T_{lm}}$ terms are symmetric and the related pressure field attains its maximum there. This distinction is useful when interpreting the spatial structure of the radiated acoustic field, since it immediately indicates which contributions are expected to dominate for observers located close to the rotor plane.

Once the coefficients A_{lm} are known, the complex acoustic pressure associated with the m-th harmonic at an observer location $\mathbf{x}_0$ is obtained from the multipole series [10]

$$p_m(\mathbf{x}_0) = \sum_{l=|m|}^{\infty} A_{lm}\, h_l(mM_t\bar{r}_0)\; Y_{lm}(\theta_0,\phi_0) \tag{3}$$

where h_l is the spherical Hankel function of the first kind and order l, and $\bar{r}_0 = r_0/R$ is the observer distance normalized by the propeller radius R. The reconstruction formula in Eq. (3) is valid only for observer locations outside the sphere enclosing the rotating lifting line, i.e. $\bar{r}_0 > 1$. The corresponding physical pressure is reconstructed from the Fourier series

$$p(\mathbf{x}_0,t) = \sum_{m=-\infty}^{\infty} p_m(\mathbf{x}_0)\, e^{-i\omega_m t} \tag{4}$$

with the condition $p_{-m}(\mathbf{x}_0) = p^*_m(\mathbf{x}_0)$.

Equation (3) is the final observer-independent representation adopted in the present work: once the multipole coefficients have been evaluated, the pressure field can be reconstructed at arbitrary observer positions without repeating the source integration. This is the key feature that makes the formulation attractive when predictions are required over large microphone sets. Since the multipole expansion is formulated independently for each harmonic m, convergence is assessed at fixed m by monitoring the truncated approximation as the maximum multipole degree $l_{\max}$ increases. The convergence of the total real pressure then follows from the Fourier reconstruction based on the converged harmonic coefficients.

When induced-velocity effects are neglected in Eq. (1), and the far-field limit of the multipole expansion is considered for Eq. (3), a direct comparison with Hanson's helicoidal-surface theory [1] becomes possible. The two formulations can be shown to be mathematically equivalent, apart from the chordwise compactness assumption adopted here. This provides a useful connection between the present observer-independent representation and a classical reference formulation for propeller tonal noise.

IV. Results

The experimental validation presented here is based on the APC propeller analysis taken from the literature [6]. The propeller is a two-bladed rotor with tip radius $R = 0.150$ m and hub radius $R_{\text{hub}} = 0.048$ m. It is characterized by a relatively slender planform, with mean chord length $c = 0.024$ m, and by a conventional linear twist distribution decreasing from approximately 33° near the root to 12° at the tip. The blade sections are based on a NACA 4412 airfoil and are assumed to be unswept. The lifting line is taken to coincide with the quarter-chord line, so that $\phi'_s(r) = c(r)/(4r)$. The aerodynamic inputs required, namely the spanwise distributions $c_l(r)$, $c_d(r)$ and $\varphi_i(r)$, are obtained from a Blade Element Momentum Theory (BEMT) computation. Results for the $n = 4000$ rpm case are shown in Fig. 1.

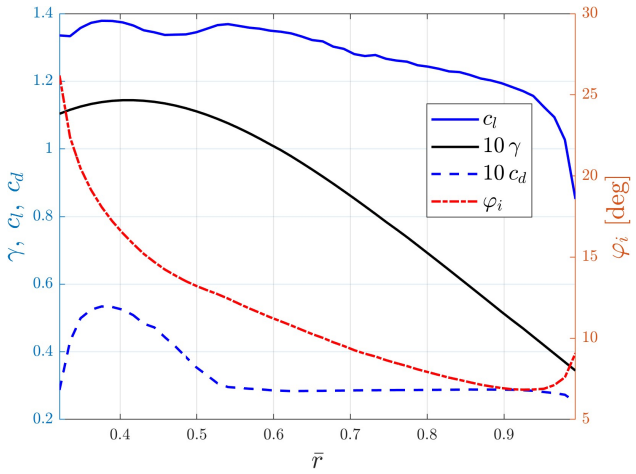

Fig. 1 Spanwise distributions of the sectional lift (c_l) and drag (c_d) coefficients, chord-to-diameter ratio (γ) and inflow angle (φ_i). The quantities c_d and γ are multiplied by 10 to improve readability on the same axis.

A. Convergence assessment of the multipole expansion

To assess the practical benefit of the observer-independent formulation, the convergence of the truncated multipole expansion was examined over extended observer regions for different operating conditions. The analysis was carried out in hovering conditions for three rotation rates, namely $n = 4000$, 5000, and 6000 rpm. For each case, the convergence study was performed in the meridional plane $\phi_0 = 0$, which contains the propeller axis and the microphone arc used in the experiments. Convergence was evaluated for the complex coefficient of the first blade-passing frequency (BPF), corresponding to $m = N$, as the truncation order $l_{\max}$ increases. This represents a favourable case for the multipole expansion because both the acoustic wavenumber and the minimum retained degree are lower than for higher harmonics. However, the first BPF is also typically the dominant tonal component in terms of radiated noise level, making it the most relevant target for assessing the practical accuracy and efficiency of the formulation. For each operating condition, a reference solution was first constructed by retaining a sufficiently large number of multipole terms, namely up to a prescribed value $l_{\max,\mathrm{ref}} = 100$. The truncation error at each observer position was measured by comparing the partial sum with the reference solution. A relative error was adopted

$$\varepsilon_m^{(l_{\max})}(\mathbf{x}_0) = \frac{\left|p_m^{(l_{\max})}(\mathbf{x}_0) - p_m^{\mathrm{ref}}(\mathbf{x}_0)\right|}{\left|p_m^{\mathrm{ref}}(\mathbf{x}_0)\right|} \tag{5}$$

Convergence was declared when $\varepsilon_m^{(l_{\max})}(\mathbf{x}_0) \le \varepsilon_{\mathrm{tol}}$, with $\varepsilon_{\mathrm{tol}}$ chosen according to the desired pressure-level accuracy. For example, if the target is an error of 0.01 dB on the harmonic sound pressure level, the corresponding relative pressure tolerance is $\varepsilon_{\mathrm{tol}} = 10^{0.01/20} - 1 \approx 0.0012$. This provides a direct spatial measure of how many terms are needed for the multipole expansion to achieve the prescribed tolerance.

The convergence maps were interpreted together with the harmonic sound pressure level associated with the reference solution. Since p_m^{ref} is the complex coefficient of the m-th harmonic, the corresponding root-mean-square pressure is $p_{m,\mathrm{rms}}(\mathbf{x}_0) = \sqrt{2}\,\left|p_m^{\mathrm{ref}}(\mathbf{x}_0)\right|$, accounting also for the conjugate $\pm m$ contributions in the real signal. The sound pressure level is therefore

$$L_{p,m}(\mathbf{x}_0) = 20\log_{10}\left(\frac{p_{m,\mathrm{rms}}(\mathbf{x}_0)}{p_{\mathrm{ref}}}\right), \qquad p_{\mathrm{ref}} = 20\ \mu\mathrm{Pa} \tag{6}$$

Plotting $L_{p,m}$ together with the minimum number of retained multipole terms to achieve convergence, i.e. $n_{\mathrm{req}} = l_{\max}^{\mathrm{req}} - m + 1$ where $l_{\max}^{\mathrm{req}}$ is the maximum l index required, makes it possible to relate convergence behaviour to the spatial structure of the radiated field.

For each rotational speed, the analysis was repeated over two observer domains in order to distinguish the behaviour of the multipole expansion in the near and far fields. Within the present framework, the far-field condition for the m-th harmonic can be expressed as $mM_t\bar{r}_0 \gg l$. Since the minimum degree is $l = |m|$, a necessary condition for far-field behaviour is therefore $\bar{r}_0 \gg \frac{1}{M_t}$. This scaling provides a convenient reference for defining the observer

regions. In the present study, the far-field domain was chosen as $[x, z] \in [0, 13.23] \times [-13.23, 13.23]$ m, which, for the 5000 rpm case, corresponds approximately to an extent of $20/M_t$. The near-field domain was instead taken as $[x, z] \in [0, 1.32] \times [-1.32, 1.32]$ m, corresponding, again for the 5000 rpm case, to an extent of approximately $2/M_t$. It should be noted that the same physical observer domains are used for all rotational speeds. As a result, their extent in normalized coordinates changes with M_t and although the geometric region is fixed, its effective position relative to the far-field transition is not the same for all cases. Since the number of terms required for convergence increases rapidly near the rotor, the contour plots are clipped at a maximum value of 11 retained terms.

Figures 2 and 3 report, for the first blade-passing harmonic $m = N$, the sound pressure level distribution in the meridional plane together with the minimum number of terms required to satisfy the prescribed convergence tolerance. Since the summation starts from $l = m$, and in the present case $m = 2$, the number of terms required in the series is simply $l_{\max}^{\text{req}} - 1$.

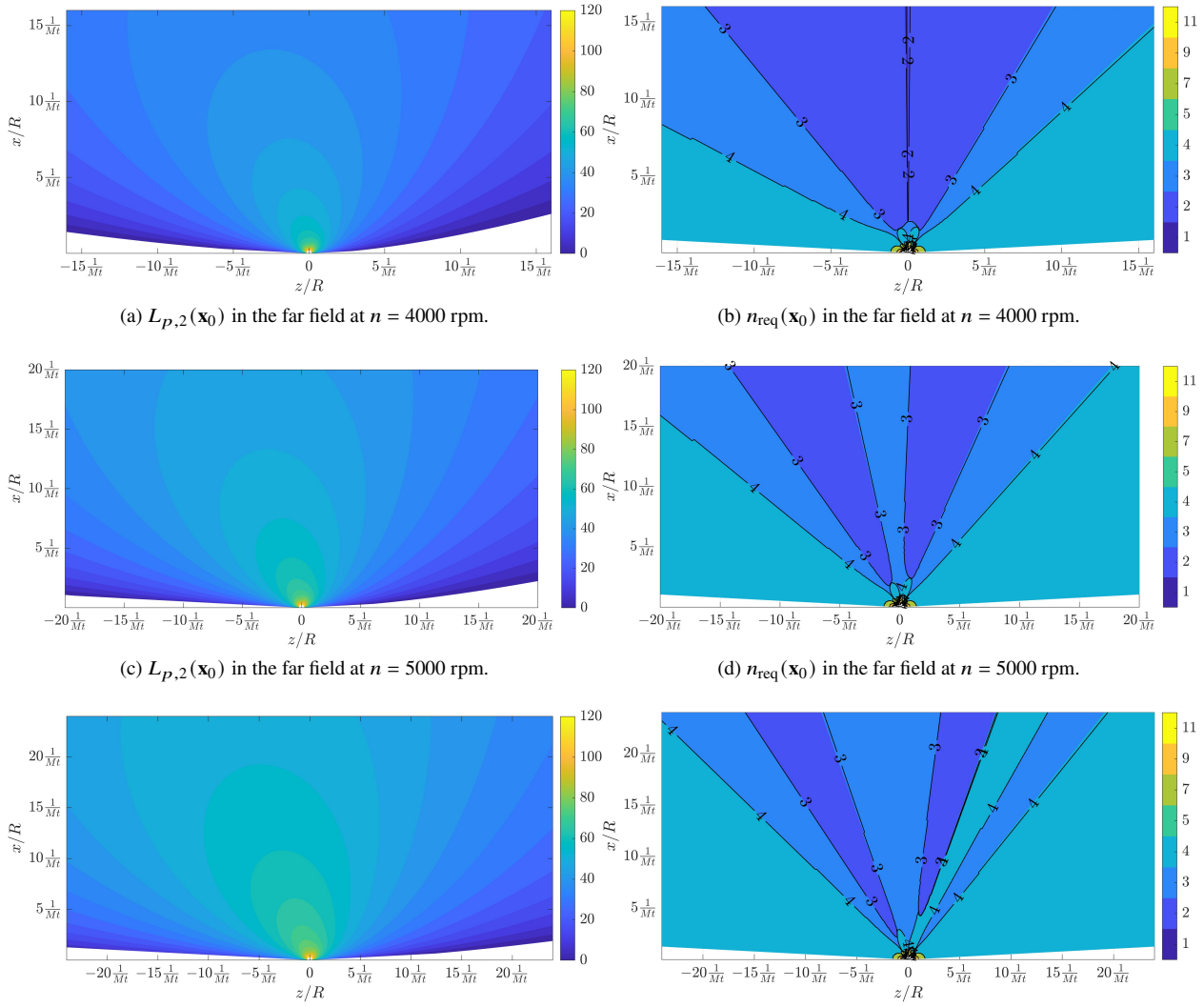

(a) $L_{p,2}(\mathbf{x}_0)$ in the far field at $n = 4000$ rpm.

(b) $n_{\text{req}}(\mathbf{x}_0)$ in the far field at $n = 4000$ rpm.

(c) $L_{p,2}(\mathbf{x}_0)$ in the far field at $n = 5000$ rpm.

(d) $n_{\text{req}}(\mathbf{x}_0)$ in the far field at $n = 5000$ rpm.

(e) $L_{p,2}(\mathbf{x}_0)$ in the far field at $n = 6000$ rpm.

(f) $n_{\text{req}}(\mathbf{x}_0)$ in the far field at $n = 6000$ rpm.

Fig. 2 Far-field maps of the first blade-passing harmonic in the meridional plane at $n = 4000$, 5000, and 6000 rpm. Left: harmonic SPL. Right: minimum number of terms required to satisfy the prescribed convergence tolerance $\varepsilon_{\text{tol}} = 0.0012$.

A first general observation is that the spatial structure of the first blade-passing harmonic remains qualitatively similar in all three cases. In both the near and far fields, the highest levels are concentrated close to the rotor and around the propeller axis, whereas the pressure decreases progressively with increasing distance from the source. As the

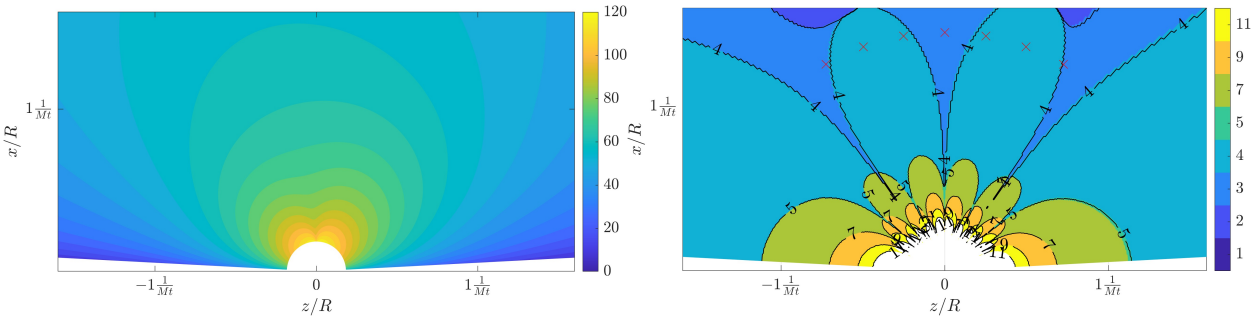

(a) $L_{p,2}(\mathbf{x}_0)$ in the near field at n = 4000 rpm.

(b) $n_{\text{req}}(\mathbf{x}_0)$ in the near field at n = 4000 rpm.

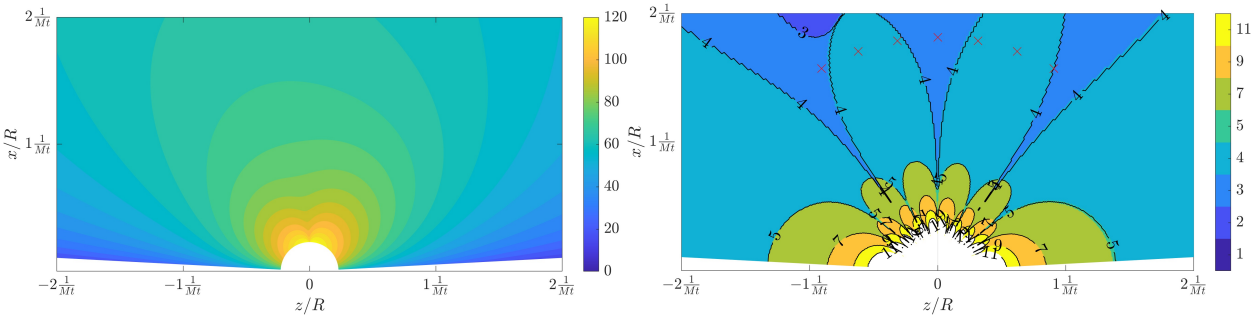

(c) $L_{p,2}(\mathbf{x}_0)$ in the near field at n = 5000 rpm.

(d) $n_{\text{req}}(\mathbf{x}_0)$ in the near field at n = 5000 rpm.

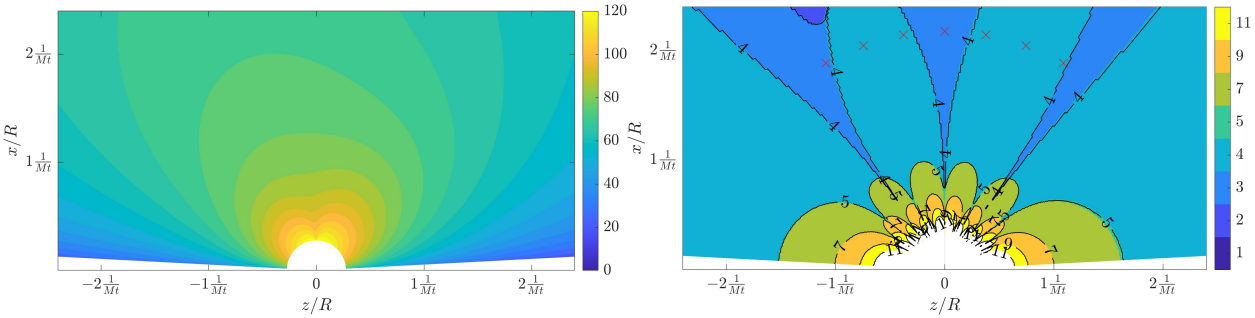

(e) $L_{p,2}(\mathbf{x}_0)$ in the near field at n = 6000 rpm.

(f) $n_{\text{req}}(\mathbf{x}_0)$ in the near field at n = 6000 rpm.

Fig. 3 Near-field maps of the first blade-passing harmonic in the meridional plane at n = 4000, 5000, and 6000 rpm. Left: harmonic SPL. Right: minimum number of terms required to satisfy the prescribed convergence tolerance $\varepsilon_{\text{tol}} = 0.0012$.

rotational speed increases from 4000 to 6000 rpm, the sound level of the harmonic increases and the region of high acoustic energy extends over a broader portion of the observer plane. At the same time, the directivity pattern remains smooth and dominated by large-scale lobes, so that the main effect of increasing rotational speed is a strengthening and spatial enlargement of the radiated field rather than a substantial change in its overall shape.

The convergence maps exhibit a similarly robust behaviour. In all cases, the largest truncation levels are required only in a relatively limited region close to the rotor, see Fig. 3, where the acoustic field varies most rapidly and the multipole expansion must reproduce its strongest spatial gradients. Away from the source, see Fig. 2, the required truncation decreases quickly, and most of the observer plane is described accurately with only a moderate number of retained terms. The largest values of n_{req} occur near the rotation axis, where the radiated pressure levels are lower and the relative-error measure is therefore more sensitive to small absolute differences between the truncated and reference solutions. Outside this region, the expansion converges rapidly and only a few terms are sufficient to recover the reference solution within the prescribed tolerance. For the operating conditions considered here, when the tolerance is relaxed from 0.01 dB to 0.1 dB, two terms are already sufficient over a wide portion of the observer region. In particular, on the rotor plane a

single term is enough, since the leading retained contribution is symmetric with respect to that plane, whereas the next one is antisymmetric and therefore vanishes there. The narrow wedge-shaped sectors observed in the far field are related to the interaction between the symmetric and antisymmetric components of the acoustic field. In regions where the lift-related contribution becomes significant, one additional multipole term is generally required to achieve convergence.

The maps also show that the required truncation increases with rotational speed, particularly in the far field, where the wedge-shaped regions broaden slightly and higher orders are needed to maintain the same accuracy. Nevertheless, even at the highest speed considered, the number of retained terms remains limited over most of the domain, confirming the practical efficiency of the proposed formulation. Moreover, the effect of increasing M_t is expected to be qualitatively similar to that of considering higher blade-passing harmonics, since m and M_t enter the expansion through their product in the acoustic wavenumber. This was verified for the second and third blade-passing harmonics, for which the far-field convergence maps show a similar behaviour, with the near-axis regions requiring higher truncation orders becoming slightly broader. When comparing the three rotational speeds, it is important to note that the same physical observation region is used in all cases. This means that the comparison is performed over the same dimensional spatial domain, but not over the same domain when distances are expressed in units of $1/M_t$. Since M_t increases with n, the characteristic scale $1/M_t$ decreases as the rotational speed increases. As a result, a fixed physical distance from the propeller corresponds to a different normalized distance for each operating condition. This is clearly reflected in the axes of the plots, where the same geometric region occupies a different extent when written in terms of $1/M_t$. The microphone locations used for the experimental comparison lie in a portion of the field where the required truncation is already moderate. This indicates that, for the present operating conditions, the observer-independent formulation can reproduce the first blade-passing harmonic at the microphone arc without requiring a large number of multipole terms.

The limited number of terms required over most of the observer domain has a direct implication for the computational cost of the method. The computational advantage of the observer-independent formulation can be estimated by comparing its cost with that of Hanson's observer-dependent formulation [1]. In the latter case, the radial source integral contains observer-dependent terms and must therefore be recomputed for each observer. If n_r is the number of radial integration points and n_o is the number of observer locations, the computational cost scales as $O(n_r + n_o + n_r n_o)$. In the present multipole formulation, the source-dependent coefficients are evaluated once for each retained degree, while the observer dependence appears only in the reconstruction step. The corresponding cost therefore scales as $O[n_{\text{req}}(n_r + n_o)]$. The resulting speed-up is $\tau_c = O\left(\frac{n_r+n_o+n_r n_o}{n_{\text{req}}(n_r+n_o)}\right)$. For the far-field convergence maps considered here, $n_r = 50$ and the rectangular observer grid contains approximately $n_o \approx 1.1 \times 10^5$ points. Taking $n_{\text{req}} \approx 3$, as representative of the truncation required over most of the far-field domain, gives $\tau_c \approx 17$, indicating a reduction of the computational cost by more than one order of magnitude for the present grid.

B. Experimental comparison

The predictive capability of the present formulation was assessed by comparison with the microphone measurements available for the hovering propeller. The comparison was carried out at the seven microphone locations placed on the arc used in the experiments, corresponding to the angular positions $\theta_0 = [60^\circ : 10^\circ : 120^\circ]$, all at the same radial distance from the rotor, corresponding to $r_0 = 8R$. The experimental values were extracted from the measured spectra at the first blade-passing harmonic and compared directly with the numerical predictions.

The resulting mean absolute error (MAE) and the root-mean-square error (RMSE) for the first blade-passing harmonic at each rpm are summarized in Table 1. The results in Fig. 4 indicate a mild overprediction in one part of the arc and a mild underprediction in the other, but with deviations that remain below 1 dB in magnitude. Overall, the comparison indicates that the proposed formulation provides an accurate prediction of the first blade-passing harmonic over the full microphone arc.

Table 1 Error metrics for the first blade-passing harmonic at the seven microphone locations.

n [rpm]	MAE [dB]	RMSE [dB]
4000	0.371	0.446
5000	0.441	0.540
6000	0.871	0.977

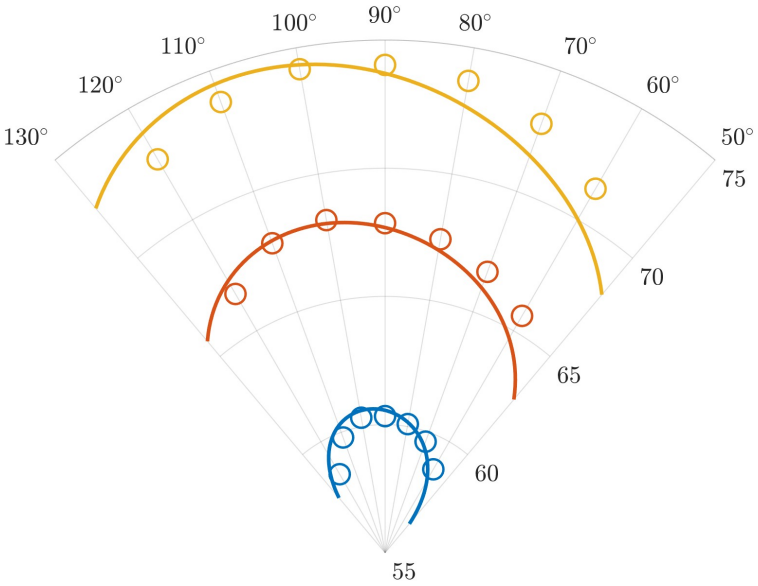

Fig. 4 Comparison between numerical and experimental sound pressure levels at the first blade-passing harmonic. The numerical prediction is shown as a continuous curve, while the measurements at the microphone locations are reported as discrete markers. The $n = 4000$ rpm case is shown in blue, the $n = 5000$ rpm case in red, and the $n = 6000$ rpm case in yellow.

C. Monte Carlo analysis

To quantify the uncertainty of the numerical prediction, a Monte Carlo analysis was performed by propagating uncertain aerodynamic, geometric, and operating inputs through the acoustic model. In each simulation, the solver evaluates the sound pressure level at the first blade-passing harmonic at the microphone locations used in the experimental comparison. The $n = 5000$ rpm case is considered.

The uncertain inputs were divided into two groups. The first group consists of spanwise distributions, namely the chord $c(\bar{r})$, the sectional lift and drag coefficients $c_l(\bar{r})$ and $c_d(\bar{r})$, and the induced-flow angle $\varphi_i(\bar{r})$. These quantities were perturbed on the fixed spanwise grid adopted by the acoustic solver. The fluctuations were modeled as correlated random fields along the blade span. More precisely, relative uncertainties were considered so that a generic quantity $v(\bar{r})$ was sampled according to

$$v(\bar{r}_k) = v_0(\bar{r}_k)\big(1 + \sigma_v z_k\big) \tag{7}$$

where v_0 is the nominal distribution, σ_v is the prescribed relative standard deviation, and z_k is the k-th component of a zero-mean correlated Gaussian random vector $\mathbf{z} = [z_1, \ldots, z_{n_{\text{span}}}]^T$. The correlation between two spanwise stations is prescribed through the covariance matrix Σ, so that

$$\mathbf{z} \sim \mathcal{N}(\mathbf{0}, \Sigma), \qquad \Sigma_{ij} = \exp\left[-\left(\frac{\bar{r}_i - \bar{r}_j}{l_{\text{corr}}}\right)^2\right]$$

where l_{corr} is the prescribed correlation length. As a result, nearby spanwise locations experience similar perturbations, while stations farther apart are less strongly correlated. It is worth noting that, with this approach, the perturbed spanwise variables are not constrained to satisfy an airfoil-polar relation. A different setting could be obtained by perturbing the underlying BEMT inputs and airfoil-polar data directly, and then recomputing the corresponding aerodynamic distributions.

The second group consists of scalar quantities, namely the rotational speed n, the air density ρ, the speed of sound a_s, and the dimensionless sectional area A_s. These were sampled independently from uniform ranges centred on their nominal values. For each realization, the corresponding set of uncertain inputs was passed to the multipole solver, which returned the SPL of the first blade-passing harmonic at the seven microphones. The uncertainty levels adopted in the Monte Carlo analysis were chosen to represent plausible uncertainty in the BEMT inputs and operating conditions, and are summarized in Table 2. Physical bounds were imposed after sampling to prevent non-admissible values of the perturbed quantities, such as negative chord, lift coefficient, drag coefficient, or inflow angle.

Table 2 Input uncertainty model adopted in the Monte Carlo analysis.

Quantity	Distribution model	Uncertainty level
$c(\bar{r})$	correlated relative Gaussian field	$\sigma_c = 0.02$
$c_l(\bar{r})$	correlated relative Gaussian field	$\sigma_{c_l} = 0.10$
$c_d(\bar{r})$	correlated relative Gaussian field	$\sigma_{c_d} = 0.10$
$\varphi_i(\bar{r})$	correlated relative Gaussian field	$\sigma_{\varphi_i} = 0.10$
n	uniform	±2%
ρ	uniform	±2%
a_s	uniform	±2%
A_s	uniform	±2%
l_{corr}	–	0.20
N_{MC}	–	1000

Figure 5 summarizes the outcome of the Monte Carlo analysis, consisting of $N_{\text{MC}} = 1000$ runs. The shaded bands denote the central 10–90% and 5–95% predictive intervals, the blue line denotes the Monte Carlo median, the black symbols the experimental values, and the red asterisks indicate the nominal prediction. The results show that the numerical model reproduces the measured directivity trend well. The nominal prediction lies almost exactly on the Monte Carlo median at all microphones, confirming that the uncertainty model is centered consistently around the baseline solution. The agreement with the measurements is very good over the first part of the arc. In particular, for microphones at $\theta_0 = 110° - 90°$ the experimental values lie essentially on the Monte Carlo median, indicating that both the level and the directivity trend are captured accurately. At $\theta_0 = 120°$ the prediction is slightly higher than the experimental mean, but the latter still lies well within the predictive interval. A modest underprediction becomes visible at the smaller elevation angles, especially at $\theta_0 = 80° - 60°$, although experimental results remain covered by the broader predictive band. Overall, the figure indicates that the remaining discrepancy is not associated with a global offset, but rather with a mild distortion of the directivity in the last part of the microphone arc. These results suggest that the uncertainty model is able to account for the experimental variability while preserving the correct overall directivity shape. At the same time, the residual mismatch observed at the smallest microphone angles indicates that additional sources of uncertainty, or a more refined aerodynamic description in that region of the field, may be needed to fully recover the measured trend there. Different values of l_{corr} were also tested. Increasing the correlation length generally led to narrower Monte Carlo uncertainty bands in the present configuration. This behaviour depends on the spatial weighting and phase variation of the acoustic integrals.

To further interpret the Monte Carlo results, a grouped uncertainty-contribution analysis was performed for the $n = 5000$ rpm case. The reference case of this analysis corresponds to the same uncertainty propagation discussed above, in which all uncertain inputs are varied simultaneously. Additional Monte Carlo runs were then carried out by perturbing one input group at a time while keeping the remaining quantities fixed at their nominal values. The groups considered were: geometry, including $c(\bar{r})$ and A_s; aerodynamic loading, including $c_l(\bar{r})$ and $c_d(\bar{r})$; inflow, including $\varphi_i(\bar{r})$; and operating conditions, including n, ρ, and a_s. Since these groups are assigned different uncertainty levels, the results should be interpreted as an uncertainty-contribution assessment under the assumptions of Table 2, rather than as an intrinsic sensitivity ranking of the acoustic model. When all inputs are perturbed simultaneously, the average standard deviation of the predicted first-BPF SPL over the microphone arc is approximately 0.82 dB. The largest individual contributions are produced by the aerodynamic loading, inflow angle, and operating-condition groups, which yield average standard deviations of approximately 0.49, 0.47, and 0.43 dB, respectively. The geometry group produces a much smaller average spread, approximately 0.13 dB, mainly because the prescribed uncertainty on the geometric quantities is smaller and because the thickness-related terms are not dominant for the present first-harmonic prediction. The single microphone results also show that the different groups do not affect all observer directions in exactly the same way: loading uncertainty is slightly more important at the larger observer angles, whereas inflow uncertainty becomes comparable to, or slightly larger than, loading at the smaller angles. This indicates that the input uncertainties affect not only the overall level but also, to a limited extent, the predicted directivity.

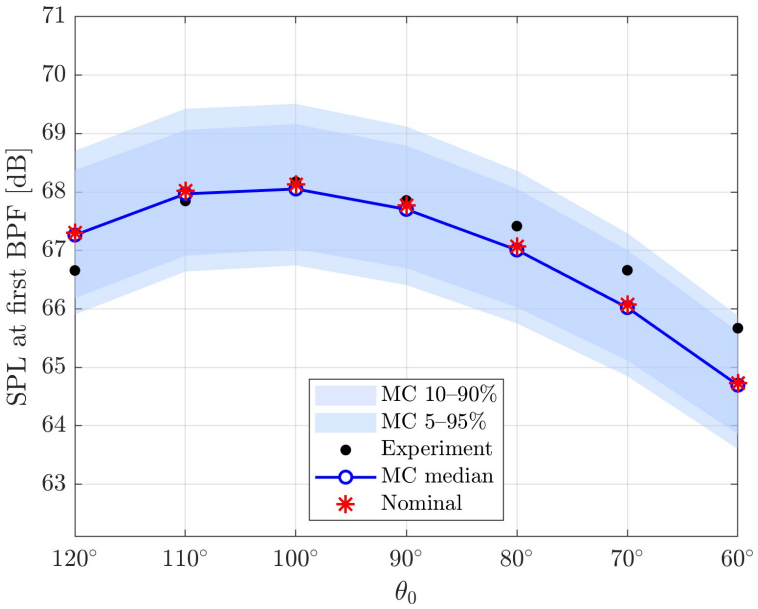

Fig. 5 Monte Carlo prediction of the SPL at the first blade-passing harmonic at the seven microphones. The shaded regions denote the central 10–90% and 5–95% predictive intervals, the blue line denotes the Monte Carlo median, the black symbols show the experimental values, and the red asterisks indicate the nominal prediction.

V. Conclusions

An observer-independent framework for the prediction of propeller tonal noise in hover has been examined, based on a spherical multipole expansion combined with a lifting-line source model. The main advantage of the formulation is the complete separation between source and observer dependence: once the multipole coefficients are evaluated, the acoustic field can be reconstructed at arbitrary observer locations without repeating the source integration. The convergence properties of the truncated multipole series were assessed for the first blade-passing harmonic. Convergence maps in the meridional plane showed that the number of retained terms required for a prescribed accuracy remains limited over most of the observer domain. The expansion converges most rapidly away from the propeller, whereas higher truncation levels are required only in restricted regions close to the rotor and along narrow sectors where the field varies more rapidly. The same analysis was repeated for different rotational speeds and for both near- and far-field observer domains. The results showed that only a modest number of terms is required in practice and that, in the far field for the rotational speeds considered here, convergence is already achieved with the first two terms of the expansion.

Validation against experimental measurements for the APC propeller confirmed the predictive capability of the formulation. The comparison at 4000, 5000, and 6000 rpm showed that the first blade-passing harmonic is reproduced accurately over the full microphone arc, with mean errors lower than 1 dB. The largest deviations were observed at the smallest microphone angles, where the numerical prediction tends to underpredict the measured levels. Nevertheless, the overall directivity trend and the level distribution were captured well in all cases. A Monte Carlo analysis was also carried out in order to quantify the effect of uncertainty in the spanwise aerodynamic and geometric inputs, as well as in the operating parameters. The results showed that the uncertainty bands remain centered around the nominal prediction and are consistent with the experimental values over most of the microphone arc. The remaining mismatch at the smallest observer angles suggests that further improvement is likely to depend more on the aerodynamic description than on the acoustic representation itself.

Overall, the present results support the use of the observer-independent multipole formulation as an accurate and efficient tool for tonal propeller-noise prediction in hovering conditions. Future work will address the extension to forward flight, the inclusion of higher-fidelity aerodynamic inputs, and the treatment of additional source mechanisms beyond the dominant tonal components considered here.

References

[1] Hanson, D. B., "Helicoidal Surface Theory for Harmonic Noise of Propellers in the Far Field," *AIAA Journal*, Vol. 18, No. 10, 1980, pp. 1213–1220. https://doi.org/10.2514/3.50873.

[2] Hanson, D. B., "Near-field frequency-domain theory for propeller noise," *AIAA Journal*, Vol. 23, No. 4, 1985, pp. 499–504. https://doi.org/10.2514/3.8943.

[3] Chapman, C. J., "The structure of rotating sound fields," *Proceedings of the Royal Society of London. Series A: Mathematical and Physical Sciences*, Vol. 440, No. 1909, 1993, pp. 257–271. https://doi.org/10.1098/rspa.1993.0015.

[4] Fruncillo, F., Luchini, P., and Giannetti, F., "A Spherical Multipole Expansion of Acoustic Analogy for Propeller Noise," , 2026. URL https://arxiv.org/abs/2603.19120.

[5] Goldstein, M., *Aeroacoustics*, Advanced book program, McGraw-Hill International Book Company, 1976.

[6] Grande, E., Ragni, D., Avallone, F., and Casalino, D., "Laminar Separation Bubble Noise on a Propeller Operating at Low Reynolds Numbers," *AIAA Journal*, Vol. 60, No. 9, 2022, pp. 5324–5335. https://doi.org/10.2514/1.J061691.

[7] Fruncillo, F., Luchini, P., and Giannetti, F., "Multipole expansion approach for rotor noise prediction," *Journal of Sound and Vibration*, Vol. 617, 2025, p. 119317. https://doi.org/10.1016/j.jsv.2025.119317.

[8] Williams, E. G., *Fourier acoustics: sound radiation and nearfield acoustical holography*, Elsevier, 1999.

[9] Brouwer, H., "On the use of the method of matched asymptotic expansions in propeller aerodynamics and acoustics," *Journal of Fluid Mechanics*, Vol. 242, 1992, pp. 117–143.

[10] Jackson, J., *Classical Electrodynamics*, Wiley, 2012.